OPAL Physics Note PN272
January 16, 1997

Search for Anomalous Production of Photonic Events with Missing Energy in e^+e^- Collisions at $\sqrt{s} = 130 - 172$ GeV

The OPAL Collaboration

Abstract

Photonic events with large missing energy have been observed in e^+e^- collisions at centre-of-mass energies between 130 and 172 GeV using the OPAL detector at LEP. Results are presented based on a new search topology which looks for photonic events with $N_\gamma \geq 2$ and significant missing energy. The selection requires at least two photons, each with scaled energy $x_\gamma > 0.05$, within the region $15° < \theta < 165°$. Analysis of the entire high-energy data sample yields 8 selected events where 11.0 are expected from the Standard Model process $e^+e^- \to \nu\overline{\nu}\gamma\gamma$. Upper limits are derived for the cross-section times branching ratio of the process $e^+e^- \to XX, X \to Y\gamma$ for $M_Y \approx 0$. Model dependent 95% CL lower limits are placed on the mass M_X for the case where X is the lightest neutralino and Y is a light gravitino. These limits assume a mean neutralino decay length much less than the inner radius of the OPAL electromagnetic calorimeter.

Results from analyses previously published for $\sqrt{s} = 130$, 136 and 161 GeV, are updated here for $\sqrt{s} = 172$ GeV. In the $\sqrt{s} = 172$ GeV data sample, corresponding to 10.5 pb^{-1}, 15 single-photon events are selected and a cross-section of 2.1$\pm$0.5 pb is measured in the kinematic acceptance, consistent with that expected for the Standard Model process $e^+e^- \to \nu\overline{\nu}\gamma(\gamma)$. In a search for acoplanar photon pairs no events are selected, yielding a 95% CL cross-section upper limit of 0.41 pb in the kinematic acceptance.

This note describes preliminary OPAL results to be submitted to the XVIII International Symposium on Lepton-Photon Interactions, Hamburg, 28 July - 1 August 1997

1 Introduction

This note describes a search for photonic events with large missing energy in e^+e^- collisions at centre-of-mass energies well above the Z^0 resonance. This includes the recent LEP data taken near $\sqrt{s} = 172$ GeV, to date the highest centre-of-mass energy achieved in e^+e^- collisions.

Three different event topologies, A, B, and C are designed to select events with one or two photons and significant transverse momentum imbalance, indicating the presence of at least one neutrino-like invisible particle which interacts only weakly with matter. The acceptance of each topology is defined in terms of the photon energy, E_γ, scaled by the beam energy, ($x_\gamma \equiv E_\gamma/E_{\mathrm{beam}}$), and the photon polar angle, θ, defined with respect to the electron beam direction. The definition of each topology is as follows :

Topology A: One or two photons accompanied by invisible particle(s) ($e^+e^- \rightarrow \gamma(\gamma)+$ invisible particle(s)). At least one photon with $x_\gamma > 0.2$ and $|\cos\theta| < 0.7$.

Topology B: Acoplanar photon pair ($e^+e^- \rightarrow \gamma\gamma+$ invisible particle(s)). Two photons each with energy exceeding 1.75 GeV and $|\cos\theta| < 0.7$.

Topology C: Events with two or more photons accompanied by invisible particle(s)). At least two photons each with $x_\gamma > 0.05$ and $15^\circ < \theta < 165^\circ$ (approximately $|\cos\theta| < 0.966$).

Search results from topology C, which is a new analysis, are presented for the entire high-energy data sample. Results from topologies A and B at $\sqrt{s} = 130 - 140$ GeV [1] and $\sqrt{s} = 161$GeV [2] have been previously published. Those results have also been used to search for excited neutrinos with photonic decays at $\sqrt{s} = 130 - 140$ GeV [3] and $\sqrt{s} = 161$ GeV [4]. These topologies are updated here for searches performed using data taken at $\sqrt{s} = 172$ GeV using selection criteria identical to those described in reference [2].

Topology A is sensitive to neutral events in which there are one or two photons and missing energy, which within the Standard Model are expected from the $e^+e^- \rightarrow \nu\bar{\nu}\gamma(\gamma)$ process. Measurements of single photon production have been made in e^+e^- collisions at the Z^0 and at lower energies [5–7]. First results from centre-of-mass energies significantly above the Z^0 mass have also been reported [1, 8]. The expected visible energies are sufficiently large at the present centre-of-mass energies that doubly radiative neutrino production can lead to two photons being detected and therefore the experimental topology includes such cases. Topology A is also sensitive to several types of new physics in e^+e^- collisions (see e.g. [5, 9] and references therein). One type of new physics is $e^+e^- \rightarrow XY$ where X decays to $Y\gamma$ and Y is an invisible particle such as a neutrino or possibly a new particle that escapes detection. One example of this type of process is production of excited neutrinos, in which case X is an excited neutrino and Y is a standard neutrino. Another example is production of neutralinos in supersymmetric theories, in which case Y is the lightest neutralino, $\tilde{\chi}^0_1$, which is stable and escapes detection, and X is a heavier neutralino, for example $\tilde{\chi}^0_2$. The branching fraction for the radiative decay, $\tilde{\chi}^0_2 \rightarrow \tilde{\chi}^0_1\gamma$, may be small, but in some cases can be dominant [10]. A related model with $X = \tilde{\chi}^0_1$ and $Y = \tilde{G}$ [11] naturally leads to a large $BR(X \rightarrow Y\gamma)$. Another type of new physics that could be seen in this search topology is the production of invisible particles made visible through initial state radiation.

Search topologies B and C are designed for neutral events with an acoplanar photon pair and significant missing energy, though topology C is designed to retain acceptance for events with a number of photons, N_γ, greater than two if the event has significant missing transverse energy. These topologies are sensitive to the production of two particles, one decaying invisibly and the other decaying into two photons. Both are sensitive also to pair production of new neutral particles each of which undergoes radiative decay to an invisible particle, i.e. $e^+e^- \to XX$, $X \to Y\gamma$. Specifically regarding the latter scenario, these topologies have acceptance for pair production of excited neutrinos ($X = \nu^*$, $Y = \nu$), and also for neutralino pair production ($X = \tilde{\chi}^0_2$, $Y = \tilde{\chi}^0_1$) for cases in which particle X can decay radiatively. The latter scenario, with a substantial photonic branching ratio, is advocated in [12]. Also of interest are models with light gravitinos, $\tilde{G}$, with $X = \tilde{\chi}^0_1$, $Y = \tilde{G}$, where the photonic branching ratio is naturally large. Such a signature has been discussed in [13] and more recently in [11, 14, 15]; cross-sections of order 1 pb are predicted at these centre-of-mass energies for $M_{\tilde{\chi}^0_1} \approx 50$ GeV.

The acceptance of topologies B and C overlap partially with that of topology A but in each case the kinematic acceptance extends well below the $x_\gamma > 0.2$ requirement of topology A, thus providing acceptance for events with very low visible energy. For topology B, which has a very low energy threshold, a more restricted angular acceptance for the second photon is imposed to reduce the generally forward-peaked backgrounds. Topology C is designed to retain as much geometric acceptance as possible while still allowing an energy threshold well below that of topology A.

All topologies are sensitive to doubly radiative neutrino production, $e^+e^- \to \nu\bar{\nu}\gamma\gamma$. This process is considered as part of the radiative correction to the inclusive single photon measurement in topology A, while for topologies B and C, it represents the essentially irreducible Standard Model background to a search for new physics processes.

This note will first briefly describe the detector, the data sample and the Monte Carlo samples used. Then the event selection for each topology will be described, followed by the results and comparison with expected Standard Model contributions. Implications of these results on the possibility of new physics processes of the type $e^+e^- \to XX$ or XY, $X \to Y\gamma$ will be discussed. This analysis is particularly sensitive for the case $M_Y \approx 0$ which is relevant to excited neutrino ($X = \nu^*$, $Y = \nu$) production and to light gravitino ($X = \tilde{\chi}^0_1$, $Y = \tilde{G}$) hypotheses.

2 Detector, Data Sample and Monte Carlo Samples

The OPAL detector is described in detail elsewhere [16]. The measurements presented here are mainly based on the observation of clusters of energy deposited in the lead-glass electromagnetic calorimeters. These calorimeters together with the gamma-catcher calorimeter, the forward calorimeters and the silicon-tungsten calorimeter provide a fully hermetic electromagnetic calorimeter down to polar angles of 33 mrad. The SiW calorimeter covers polar angles down to 24 mrad, however the region around 30 mrad lacks useful calorimetric coverage due to the installation in 1996 of a thick tungsten shield designed to protect the tracking chambers from accelerator backgrounds at LEP2 energies. The tracking system, consisting of a silicon microvertex detector, a vertex drift chamber and a large volume jet drift chamber, is used to select events consistent with zero charged particle multiplicity. Backgrounds from cosmic-ray interactions are removed using time-of-flight (TOF) information, the hadron calorimeter and muon detectors.

The data used in this analysis were recorded at e^+e^- centre-of-mass energies of 130.3, 136.2, 161.3, and 171.8 GeV[1], with integrated luminosities of 2.6, 2.5, 10.0, and 10.5 pb^{-1}, respectively. For topologies A and B, results are presented here for only the $\sqrt{s} = 171.8$ GeV data. The integrated luminosities are determined to better than 1% from small angle Bhabha scattering events in the silicon-tungsten luminosity calorimeter.

For the expected Standard Model signal process of $e^+e^- \to \nu\bar{\nu}\gamma(\gamma)$, the Monte Carlo generator NUNUGPV [17] was used. For the expected Standard Model background processes, we used a number of different generators: RADCOR [18] for $e^+e^- \to \gamma\gamma(\gamma)$; BHWIDE [19] and TEEGG [20] for $e^+e^- \to$

[1]This value represents the luminosity-weighted mean $\sqrt{s}$ of data taken at $\sqrt{s} = 170.0$ and $\sqrt{s}$=172.0.

$e^+e^-(\gamma)$; KORALZ [21] for $e^+e^- \to \mu^+\mu^-(\gamma)$ and $e^+e^- \to \tau^+\tau^-(\gamma)$; and the Vermaseren program [22] for leptonic final states from two-photon collisions.

To simulate possible new physics processes of the type $e^+e^- \to XY$ and $e^+e^- \to XX$ where X decays to $Y\gamma$ and Y escapes detection, the SUSYGEN [23] Monte Carlo generator was used. We produced neutralino pair events of the type $e^+e^- \to \tilde{\chi}^0_2\tilde{\chi}^0_1$ and $e^+e^- \to \tilde{\chi}^0_2\tilde{\chi}^0_2$, where $\tilde{\chi}^0_2 \to \tilde{\chi}^0_1\gamma$. Using the relatively flat angular distribution observed in the production of these generated events, the estimated efficiencies are generalized to the generic processes (replacing $\tilde{\chi}^0_2$ with X and $\tilde{\chi}^0_1$ with Y), assuming an isotropic angular distribution for XY and XX production and for X decay. For this note we used samples of XY production with M_X from 80 to 160 GeV and with $M_Y = 0$. For XX production we used SUSYGEN $\tilde{\chi}^0_2\tilde{\chi}^0_2$ samples with M_X from 45 to 80 GeV and $M_Y = 0$ and OPAL excited neutrino Monte Carlo [4] with M_X from 45 to 85 GeV. The efficiencies for XX and XY production, obtained from analysis of the SUSYGEN Monte Carlo samples for the case $M_Y = 0$, are found to be consistent within statistical errors with the efficiencies obtained using the OPAL excited neutrino Monte Carlo.

All the above Monte Carlo samples were processed through the OPAL detector simulation [24].

3 Event Selection Description

3.1 Topology A: Events with one or two photons and invisible particle(s)

Events are selected as having one or two photon candidates if they satisfy the following criteria based on previous OPAL analyses of photonic events with missing energy [1,2,5,25]:

- **Charged track veto.** Events are required to have no tracks with 20 or more jet chamber hits assigned to them, reconstructed in the central detector.
- **Angular acceptance and minimum energy.** An event is considered to contain a photon candidate if the primary electromagnetic cluster (that with the highest deposited energy in the barrel and endcap calorimeters) is in the region $|\cos\theta| < 0.7$ and has a scaled energy, x_γ, that exceeds 0.2. Events are considered to have more than one photon if additional electromagnetic clusters are found in the barrel or endcap calorimeter ($|\cos\theta| < 0.984$) having deposited energy exceeding 300 MeV. Acceptance for events with two photons is desirable in order to increase the efficiency for doubly radiative neutrino production, and so reduce the sensitivity to the modelling of that process.
- **Cluster extent.** The primary electromagnetic cluster combined with any clusters contiguous with it must not extend more than 250 mrad (equivalent to more than six lead-glass blocks) in the polar or azimuthal directions. It must also consist of at least two blocks.
- **Coil conversion seen in TOF system.** The primary electromagnetic cluster must be matched within 50 mrad in azimuthal angle by a good quality TOF counter signal produced by the photon converting in the coil in front of the TOF. The measured arrival time of the photon at the TOF must be within 20 ns of the expected time for a photon originating from the interaction point.
- **Forward calorimeter veto.** The total energy deposited in each forward calorimeter must be less than 2 GeV.
- **Gamma-catcher veto.** The most energetic gamma-catcher cluster must have an energy of less than 5 GeV. The forward calorimeter veto and gamma-catcher veto serve to ensure that photon candidate events are not accompanied by any event activity in the forward regions.

- **Muon veto.** Events are rejected if there are any muon track segments reconstructed in the barrel or endcap muon chambers, or in the barrel, endcap or pole-tip hadron calorimeters. Events are also rejected if three or more of the outer 8 layers of the barrel hadron calorimeter have strips hit in any 45° azimuthal road. The muon veto is used primarily to remove cosmic ray background.

Background from $e^+e^- \to \gamma\gamma(\gamma)$ is rejected if any of the following criteria are satisfied for events with a second cluster:

- The total energy of the two clusters exceeds 90% of the centre-of-mass energy.
- The acoplanarity angle of the two clusters[2], ϕ_{acop}, is less than 2.5°.
- The missing momentum vector calculated from the two clusters satisfies $|\cos\theta_{\mathrm{miss}}| > 0.9$.
- A third electromagnetic cluster is detected with deposited energy exceeding 300 MeV.

3.2 Topology B: Events with an acoplanar photon pair and invisible particle(s)

The event selection for this topology is also based on the previous OPAL analyses described in references [1, 2] and [26]. The selection criteria for topology B are identical to those of topology A except for the following two requirements:

- **Angular acceptance and minimum energy.** Candidate events are required to contain two electromagnetic clusters in the calorimeter, both having deposited energy exceeding 1.5 GeV and detected in the region $|\cos\theta| < 0.7$. Following [5], the experimental requirement on deposited energy exceeding 1.5 GeV corresponds to an effective minimum photon energy of 1.75 GeV. The cluster with the higher energy must pass the cluster extent criteria of topology A.
- **Coil conversion seen in TOF system.** At least one electromagnetic cluster must be matched within 50 mrad in azimuthal angle with a good quality TOF counter signal. The measured arrival time of the photon at the TOF must be within 20 ns of the expected time for a photon originating from the interaction point.

The restricted angular acceptance for the two photons in topology B not only discriminates against forward-peaked background, it also ensures precise measurement of the photon energies and helps ensure that time-of-flight information is available to check that the photons are consistent with originating from the interaction point. Background events, coming principally from $e^+e^- \to \gamma\gamma(\gamma)$, are rejected if any of the same four veto conditions described in topology A are satisfied.

3.3 Topology C: Photonic events with $N_\gamma \geq 2$ and invisible particle(s)

The event selection for this topology is based on the previous OPAL analysis described in reference [1]. In that paper, however, this topology was used simultaneously as a search analysis and for measurement of the Standard Model cross-section for the QED process $e^+e^- \to \gamma\gamma(\gamma)$, within the kinematic acceptance of the analysis. The measurement of the QED cross-section at higher energies will be described later in a separate note. In this note selection criteria are modified to suppress background from this source. Acceptance is retained for events with more than two photons if they have significant transverse missing energy. The selection criteria are otherwise similar to those described in reference [1]. However since a number of modifications have been made to increase efficiency for the

[2] Defined as 180° minus the opening angle in the transverse plane.

signal events of interest and to lower the energy threshold, the selection criteria are described in detail below.

Firstly, we select events with at least two electromagnetic clusters with x_γ exceeding 0.05 and each having a polar angle in the range $15^\circ < \theta < 165^\circ$.

We use selection criteria designed to reject events having tracking information consistent with the presence of at least one charged particle originating from the interaction point. This is done in such a way as to retain acceptance for events in which one or both of the photons convert. These charged track vetos are implemented as in the topology C analysis in reference [1].

In order to suppress backgrounds arising from cosmic-ray muon interactions or beam halo muons which can deposit significant energy in the calorimeter, the events must pass the muon veto described for topology A. Additionally, events are vetoed if they produced a muon trigger [28].

For events in which both of the photon candidates lie within $|\cos\theta| < 0.82$, at least one of them must pass the TOF requirement described above for the highest-energy photon in Topology A. In the case where only one of the two photons lies in the barrel region, TOF information is not required. However, if such information is present it is required to be consistent with the expected photon timing. Finally, if there is a charged track associated with a cluster within the polar region $|\cos\theta| < 0.82$, the requirement of good TOF with consistent timing is applied.

Additional suppression of cosmic, beam-related and instrumental backgrounds is obtained by imposing the following requirements:

- Events are vetoed if there is more than one charged track with at least 40 hits in the jet chamber and an unconstrained $|z_0|$ larger than 100 cm. This suppresses beam halo and beam wall/beam gas events.
- Events are vetoed if there are more than 5 ECAL clusters, each with more than 1 GeV of deposited energy. This suppresses events in which a cosmic or beam halo muon grazes the electromagnetic calorimeter.
- The opening angle ψ of the two-photon system is required to satisfy $\cos\psi < 0.99$.

The forward vetoes described for topology A are applied with thresholds of 5 GeV for both the forward calorimeter and the gamma-catcher. An additional forward veto requires that the total energy deposited in the each silicon-tungsten calorimeter be less than 5 GeV.

Background from $\mathrm{e^+e^-} \to \gamma\gamma(\gamma)$ is rejected if any of the following criteria are satisfied:

- The total visible energy of the event is greater than $0.95\sqrt{s}$.
- The acoplanarity, ϕ_{acop}, of the two highest-energy clusters is less than 2.5°.
- The missing momentum vector calculated from the two highest-energy clusters satisfies $|\cos\theta_{\mathrm{miss}}| > 0.95$.
- Events having a third photon candidate (with $x_\gamma > 0.05$) are rejected unless the three photon system is significantly non-coplanar (sum of the three opening angles $< 350^\circ$) and has significant net scaled transverse momentum $\Sigma_i p_t(\gamma_i)/E_{\mathrm{beam}} > 0.1$.

4 Results

4.1 Topology A

After applying the selection criteria of topology A to the $\sqrt{s} = 172$ GeV data sample, 15 events are selected. From the Monte Carlo we expect a Standard Model signal from $e^+e^- \to \nu\overline{\nu}\gamma(\gamma)$ of 13.5 ± 0.3 events. The selection efficiency for this Standard Model process is (67 ± 1) % for generated events within the kinematic acceptance (i.e. at least one photon with $x_\gamma > 0.2$ and $|\cos\theta| < 0.7$). Most of the inefficiency arises when a photon either converts in the tracking volume, or does not convert until it enters the lead glass calorimeter. In the former case, such events are vetoed by the presence of charged tracks and in the latter case it is unlikely that a TOF hit will be associated with the electromagnetic cluster.

Here and throughout the paper the quoted errors on efficiencies include estimates of the systematic errors which are small compared to the statistical errors on the measurements. The expected $e^+e^- \to \nu\overline{\nu}\gamma(\gamma)$ contribution is composed of 11.3 ± 0.3 single photon events and 2.2 ± 0.1 two photon events (see Table 1). In the data 13 events are single photon events and two events are two photon events. The expected contributions from other Standard Model background processes are estimated to be negligible (less than 0.1 events expected). Beam-related, cosmic ray and instrumental background contributions are also negligible. With 15 observed events, correcting for the selection efficiency yields a cross-section for $e^+e^- \to \nu\overline{\nu}\gamma(\gamma)$ within the kinematic acceptance of topology A of 2.1 ± 0.5 pb, consistent with the Standard Model prediction of 1.9 pb. This measured cross-section, along with the corresponding OPAL measurements at $\sqrt{s}$=130, 136, and 161 GeV are plotted in Fig. 1. The curve shows the predicted Standard Model cross-section.

The scaled energy distribution of the most energetic photon for events found in the data is plotted along with the expected Standard Model signal $e^+e^- \to \nu\overline{\nu}\gamma(\gamma)$ and background contributions in Fig. 2a. In the figure, the threshold for the x_γ cut has been lowered to 0.025 (about 2 GeV) to show the expected background contributions at low photon energy. There is good agreement between data and Monte Carlo predictions both for the background dominated low x_γ region and in the $x_\gamma > 0.2$ signal region. That the 15 selected events in the data are consistent with the expectation for $e^+e^- \to \nu\overline{\nu}\gamma(\gamma)$ can also be seen in the distribution of the mass recoiling against the photon (or two-photon system) as shown in Fig. 2b. One expects a peak in the recoil mass at M_Z, since the $\nu\overline{\nu}$ predominantly comes from the decay of a Z^0.

Applying a cut on the recoil mass of $M_{rec} < 75$ GeV and requiring only one photon, removes most of the Standard Model $e^+e^- \to \nu\overline{\nu}\gamma(\gamma)$ events, providing a nearly background-free kinematic region to look for possible new physics processes. The number of events from $e^+e^- \to \nu\overline{\nu}\gamma(\gamma)$ expected from the Monte Carlo is reduced from 13.5 to 0.11 after the first cut and further reduced to 0.05 after the second. No events survive the first cut in the data. This yields a 95% CL upper limit of 0.43 pb for single photon production within this kinematic region. This limit uses the expected polar angle and energy distributions for the process $e^+e^- \to \nu\overline{\nu}\gamma(\gamma)$ but is not very sensitive to the shape of these distributions. The systematic error is incorporated into all limits quoted in this paper using the method described in [29].

After applying the topology A selection with the additional two cuts described above, we obtain the efficiency for selecting events from the process $e^+e^- \to XY, X \to Y\gamma$ ($M_Y \approx 0$), which varies from 12% for $M_X = 80$ GeV to 53% for $M_X = 170$ GeV as shown in Table 2. Based on these efficiencies and on no observed events in the data, we can set an upper limit on the cross-section times photonic branching ratio, $\sigma_{XY}\times$ BR($X \to Y\gamma$), of 0.5 to 2.5 pb depending on M_X, as shown in Fig. 3. This limit applies to the supersymmetry process of $\tilde{\chi}^0_2\tilde{\chi}^0_1$ production where $\tilde{\chi}^0_1$ is massless, to the case of single production of excited neutrinos ($e^+e^- \to \nu^*\nu,\ \nu^* \to \nu\gamma$) and to the case of $\tilde{\chi}^0_1\tilde{G}$ production.

4.2 Topology B

After applying the selection criteria of topology B to the $\sqrt{s} = 172$ GeV data sample, no events remain, consistent with the expectation for the Standard Model process $e^+e^- \to \nu\overline{\nu}\gamma\gamma$ of 0.71 ± 0.06 events. The expected number of events from other processes and instrumental backgrounds is negligible. The selection efficiency for this process is (71 ± 3) % for those events generated within the kinematic acceptance of topology B (i.e., both photons having $E_\gamma > 1.75$ GeV and $|\cos\theta| < 0.7$). This information is summarized in Table 3. We set an upper limit on the cross-section within this kinematic acceptance for acoplanar photon pair production of 0.41 pb at 95% CL. This limit uses the expected polar angle and energy distributions for the process $e^+e^- \to \nu\overline{\nu}\gamma\gamma$ but is not very sensitive to the shape of these distributions. The expected cross-section for $e^+e^- \to \nu\overline{\nu}\gamma\gamma$ is 0.10 pb.

4.3 Topology C

After applying the selection criteria of topology C to all of the high-energy data, a total of 8 events are seen, where 11.0 ± 0.2 events are expected from the Standard Model process $e^+e^- \to \nu\overline{\nu}\gamma\gamma$. Contributions from other Standard Model processes are negligible. Instrumental backgrounds were found not to be significant. Additionally, all selected events were graphically scanned and determined to be consistent with the $e^+e^- \to \nu\overline{\nu}\gamma\gamma$ process. The breakdown of the observed and expected number of events for the different centre-of-mass energies is given in Table 4. There were no selected events having $N_\gamma > 2$. The results of the analyses are shown for each centre-of-mass energy region in Figs. 4-6. For each figure (a) shows the distribution of the scaled energy of the least energetic photon candidate, x_2; (b) shows the recoil mass distribution; (c) shows the polar angle distribution for the least energetic photon; (d) shows the scaled energy of the least energetic photon (x_2) plotted against the scaled energy of the most energetic photon (x_1). In (a)-(c) the histograms represent the expected distributions from $e^+e^- \to \nu\overline{\nu}\gamma\gamma$, normalized in each case to the corresponding integrated luminosity. In (d) the $\nu\overline{\nu}\gamma\gamma$ distribution is shown as small points and is not normalized. In the recoil mass distributions the events are clustered about the mass of the Z^0 as is expected for events from the process $e^+e^- \to \nu\overline{\nu}\gamma\gamma$.

Recently, interest has been rekindled in models in which the lightest supersymmetric particle is a light gravitino [11, 14, 15]. In such models, events with acoplanar photon pairs arise via $\tilde{\chi}^0_1$ pair production followed by the decays $\tilde{\chi}^0_1 \to \tilde{G}\gamma$. One can calculate [14] the maximum and minimum neutralino masses, M_X^{max} and M_X^{min}, which are consistent with the kinematic properties of the two photons, assuming a massless gravitino. As this argument is based only on kinematics it applies generally to the case where the acoplanar photon pair originates from pair production of heavy neutral particles which decay photonically to massless invisible final states; $e^+e^- \to XX$ followed by $X \to Y\gamma$, $M_Y \approx 0$. These maximum and minimum mass values can be used to suppress the $\nu\overline{\nu}\gamma\gamma$ background while retaining high efficiency for the signal hypothesis. Fig. 7 shows M_X^{min} vs. M_X^{max} for events passing the selection criteria described in section 3.3 for, (a) $\nu\overline{\nu}\gamma\gamma$ Monte Carlo and (b-f) $e^+e^- \to XX, X \to Y\gamma, M_Y = 0$ signal Monte Carlo, each at $\sqrt{s} = 161$ GeV. The signal Monte Carlo distributions are dominantly populated at maximum mass values greater than or equal to the generated mass of the heavy neutral (*e.g.* ν^* or $\tilde{\chi}^0_1$). Requiring that the maximum kinematically allowed mass be greater than $M_X - 5$ GeV provides an additional suppression of 46% to 94% for the $\nu\overline{\nu}\gamma\gamma$ background, while retaining better than 90% relative efficiency for signal at all values of M_X.

The kinematic properties of the events selected by the topology C analysis, including the values of M_X^{max}, are provided in Table 5. The data distributions in M_X^{min} vs. M_X^{max} are shown for each of the centre-of-mass energies in Fig. 8. In each case the distribution for $\nu\overline{\nu}\gamma\gamma$ events is also shown. For illustrative purposes, the efficiencies calculated from Monte Carlo events generated at 161 GeV are shown in Table 6 before and after application of the cut on M_X^{max}. Also shown is the $\nu\overline{\nu}\gamma\gamma$ rejection efficiency obtained with the M_X^{max} cut. Signal efficiencies at other centre-of-mass energies are similar.

To maintain consistency with the M_X^{max} cut described above, in the data analysis candidates are considered to be consistent with the $e^+e^- \to XX, X \to Y\gamma$, $M_Y \approx 0$ scenario for M_X values up to $M_X^{max} + 5$ GeV. Fig. 9 shows the number of selected data events consistent with a given mass value M_X, for the data samples at each of the three centre-of-mass regions. Overlaid in each case is the expected number of background events from $\nu\bar{\nu}\gamma\gamma$ events. From these distributions and the efficiencies we calculate a 95% CL upper limit on $\sigma_{XX} \times BR^2(X \to Y\gamma)$ (for $M_Y \approx 0$) as a function of M_X. These are shown in Fig. 10. These limits are calculated in the manner described in [30] for the observation of N_{obs} events where N_{bkg} background events are expected. The limits are set conservatively; where the number of observed events is less than the expected background level, the limit is calculated using $N_{bkg} = N_{obs}$.

To set a limit from the combined high-energy data sample, we sum the number of observed events consistent with each value of M_X as well as the expected number of events from $\nu\bar{\nu}\gamma\gamma$ as a function of M_X. These distributions are shown in Fig. 11 where the solid line shows the number of observed candidates consistent with a given value of M_X and the dotted line shows the background expectation. The dashed line shows the 95% confidence level upper limit at each mass value. The limits are calculated as described above. Also shown in Fig. 11 is the number of events expected from the Lopez and Nanopoulos no-scale supergravity model [14]. Based on these distributions, that model is ruled out at the 95% confidence level for $M_{\tilde{\chi}_1^0} < 72.3$ GeV. Fig. 12 shows the same limit distribution compared to the model of Babu, Kolda and Wilczek [15] in which X is again the lightest neutralino, χ_1^0, Y is again a light gravitino, and the neutralino composition is purely gaugino (bino). This model is ruled out at the 95% CL for $M_{\tilde{\chi}_1^0} < 73.8$ GeV.

As described above, the efficiencies over the full angular range have been calculated with isotropic angular distributions for production and decay of X. The validity of this assumption has been examined based on the angular distributions calculated for photino pair production in [13]. For models proposed in [11], the production angular distributions are more central and so this assumption is conservative. For an extreme case, namely a $1 + \cos^2\theta$ production angular distribution, appropriate to t-channel exchange of a very heavy particle [13], the relative efficiency reduction would be at most 2%. We have evaluated the efficiency with zero decay length for X; efficiencies are unaffected if the decay length is much less than the inner radius of the barrel electromagnetic calorimeter (2.5 m).

5 Conclusions

We have searched for photonic events with large missing energy in three different and complementary topologies in data taken with the OPAL detector at LEP at centre-of-mass energies well above the Z^0 resonance.

In the topology A selection at $\sqrt{s} = 172$ GeV which requires events having at least one photon with $x_\gamma > 0.2$ and $|\cos\theta| < 0.7$, 15 events are observed in the data compared to an expected contribution from the Standard Model process $e^+e^- \to \nu\bar{\nu}\gamma(\gamma)$ of 13.5 ± 0.3. This corresponds to a cross-section for $e^+e^- \to \nu\bar{\nu}\gamma(\gamma)$ of 2.1 ± 0.5 pb in the kinematic acceptance of topology A, consistent with the Standard Model prediction of 1.9 pb. By considering only events with a single photon and with a recoil mass below 75 GeV, based on no observed events, we determine a 95% CL upper limit for the cross-section of 0.43 pb. In addition we set an upper limit on the cross-section times photonic branching ratio for the process $e^+e^- \to XY, X \to Y\gamma, M_Y \approx 0$ as a function of M_X. This limit is of particular interest for the case of new physics processes producing single photons such as for the supersymmetry process $e^+e^- \to \tilde{\chi}_2^0\tilde{\chi}_1^0 \to \tilde{\chi}_1^0\tilde{\chi}_1^0\gamma$ and for single production of excited neutrinos.

The topology B selection, also at $\sqrt{s} = 172$ GeV, which requires events having two photons, each with energy exceeding 1.75 GeV and $|\cos\theta| < 0.7$, finds no events passing all cuts. This is also consistent with the prediction for the Standard Model process $e^+e^- \to \nu\bar{\nu}\gamma(\gamma)$ of 0.71 ± 0.06 events.

We set an upper limit on the cross-section for acoplanar photon pair production in the kinematic acceptance of topology B of 0.41 pb at 95% confidence level.

In topology C, which is similar to topology B but with improved angular acceptance at the small cost of some low energy acceptance, a total of 8 events are observed in the entire high-energy data sample ($\sqrt{s}$ =130, 136, 161, 172 GeV). A total of 11.0 ± 0.2 events are expected from the Standard Model process $e^+e^- \rightarrow \nu\bar{\nu}\gamma\gamma$. At each centre-of-mass energy we set model independent upper limits on the cross-section times photonic branching ratio squared for the process $e^+e^- \rightarrow XX, X \rightarrow Y\gamma$ for the case where $M_Y \approx 0$. These limits are of particular interest for new physics processes producing acoplanar photon pairs and undetectable massless particles, for example, pair produced neutralinos, where the neutralino decays into a photon and a light gravitino, or pair produced excited neutrinos.

A combined limit obtained from the topology C analysis of all the high-energy data is formed by summing the data and background expectation distributions obtained at different centre-of-mass energies. For the process $e^+e^- \rightarrow XX$ followed by $X \rightarrow Y\gamma$, $M_Y \approx 0$. We derive a combined upper limit on the number of candidates consistent with M_X between 45 and 86 GeV. Comparing this with the expected number of events from the model predictions of Lopez and Nanopoulos [14] permits exclusion of that model for M_X values up to 72.3 GeV. A similar model [15] is excluded for $M_X < 73.8$ GeV.

6 Acknowledgements

The authors wish to thank J.L. Lopez for providing cross-section results.

References

[1] OPAL Collab., G. Alexander et al., Phys. Lett. **B377** (1996) 222.

[2] OPAL Collab., K. Ackerstaff et al., CERN-PPE/96-154, to be published in Phys. Lett. B.

[3] OPAL Collab., G. Alexander et al., Phys. Lett. **B386** (1996) 463.

[4] OPAL Collab., K. Ackerstaff et al., CERN-PPE/96-138, to be published in Phys. Lett. B.

[5] OPAL Collab., R. Akers et al., Z. Phys. **C65** (1995) 47.

[6] L3 Collab., B. Adeva et al., Phys. Lett. **B275** (1992) 209;
L3 Collab., O. Adriani et al., Phys. Lett. **B292** (1992) 463;
ALEPH Collab., D. Buskulic et al., Phys. Lett. **B313** (1993) 520;
DELPHI Collab., P. Abreu et al., CERN-PPE/96-03, submitted to Z. Phys. **C**.

[7] MAC Collab., W.T. Ford et al., Phys. Rev. **D33** (1986) 3472;
H. Wu, Ph.D Thesis, Univ. Hamburg, 1986;
CELLO Collab., H.-J. Behrend et al., Phys. Lett. **B215** (1988) 186;
ASP Collab., C. Hearty et al., Phys. Rev. **D39** (1989) 3207;
VENUS Collab., K. Abe et al., Phys. Lett. **B232** (1989) 431;
TOPAZ Collab., T. Abe et al., Phys. Lett. **B361** (1995) 199.

[8] ALEPH Collab., D. Buskulic et al., Phys. Lett. **B384** (1996) 333;
L3 Collab., M. Acciarri et al., Phys. Lett. **B384** (1996) 323;
DELPHI Collab., P. Abreu et al., Phys. Lett. **B380** (1996) 471.

[9] L3 Collab., M.Acciarri et al., Phys. Lett. **B346** (1995) 190 and Phys. Lett. **B350** (1995) 109.

[10] H.E. Haber and D. Wyler, Nucl. Phys. **B323** (1989) 267;
S. Ambrosanio and B. Mele, Phys. Rev. **D53** (1996) 2541.

[11] S. Dimopoulos et al., Phys. Rev. Lett. **76** (1996) 3494;
D.R. Stump, M. Wiest, C.P. Yuan, Phys. Rev. **D54** (1996) 1936;
S. Ambrosanio et al., Phys. Rev. **D54** (1996) 5395.

[12] S. Ambrosanio et al., Phys. Rev. Lett. **76** (1996) 3498 and hep-ph/9607414.

[13] J. Ellis and J.S. Hagelin, Phys. Lett. **B122** (1983) 303.

[14] J.L. Lopez and D.V. Nanopoulos, Mod. Phys. Lett. **A11** (1996) 2473;
J.L. Lopez, D.V. Nanopoulos, A. Zichichi, Phys. Rev. Lett. **77** (1996) 5168.

[15] K. S. Babu, C. Kolda and F. Wilczek, Phys. Rev. Lett **77** (1996) 3070;
C.Y. Chang and G.A. Snow, UMD/PP/96-57.

[16] OPAL Collab., K. Ahmet et al., Nucl. Instrum. Methods **A305** (1991) 275;
P.P. Allport et al., Nucl. Instrum. Methods **A324** (1993) 34;
P.P. Allport et al., Nucl. Instrum. Methods **A346** (1994) 476;
B.E. Anderson et al., IEEE Transactions on Nuclear Science **41** (1994) 845.

[17] G. Montagna et al., Nucl. Phys. **B452** (1996) 161;
G. Montagna, O. Nicrosini and F. Piccinini, FNT/T-96/1, to be published in Comp. Phys. Comm.

[18] F.A. Berends and R. Kleiss, Nucl. Phys. **B186** (1981) 22.

[19] S. Jadach, W. Placzek and B. F. L. Ward, University of Tennessee preprint, UTHEP 95-1001 (unpublished).

[20] D. Karlen, Nucl. Phys. **B289** (1987) 23.

[21] S. Jadach et al., Comp. Phys. Comm. **66** (1991) 276.

[22] J. A. M. Vermaseren, Nucl. Phys. **B229** (1983) 347.

[23] S. Katsanevas and S. Melachronios, CERN/96-01, Vol.2 (1996) 328.

[24] J. Allison et al., Nucl. Instrum. Methods **A317** (1992) 47.

[25] OPAL Collab., G. Alexander et al., Phys. Lett. **B377** (1996) 273.

[26] OPAL Collab., P.D. Acton et al., Phys. Lett. **B311** (1993) 391.

[27] K. Sachs OPAL Physics Note in progress.

[28] M. Arignon et al., Nucl Instrum. Methods **A313** (1992) 103.
The relevant triggers are MBH,MEL,MER.

[29] R. D. Cousins and V. L. Highland, Nucl. Instrum. Methods **A320** (1992) 331.

[30] Particle Data Group, R. M. Barnett et al., Phys. Rev. **D54** (1996) 1.

Process	1 photon	1 or 2 photons	1 photon and $M_{rec} < 75$ GeV	1 or 2 photons and $M_{rec} < 75$ GeV
Data	13	15	0	0
$e^+e^- \to \nu\overline{\nu}\gamma(\gamma)$	11.3 ± 0.3	13.5 ± 0.3	0.05 ± 0.02	0.11 ± 0.02

Table 1: Topology A selection: Number of events observed in the data and expected number of events from the process $e^+e^- \to \nu\overline{\nu}\gamma(\gamma)$ for an integrated luminosity of 10.5 pb^{-1}.

M_X (GeV)	Efficiency in % for topology A selection	Efficiency in % for topology A with 1 photon and $M_{rec} < 75$ GeV
80	52 ± 2	12 ± 1
110	51 ± 2	16 ± 1
140	52 ± 2	27 ± 1
170	53 ± 2	53 ± 2

Table 2: Topology A selection efficiency as a function of mass for the process $e^+e^- \to XY$, $X \to Y\gamma$, and $M_Y \approx 0$.

Process	standard selection	
	effic. in %	no. of events
Data		0
$e^+e^- \to \nu\overline{\nu}\gamma\gamma$	71 ± 3	0.71 ± 0.06

Table 3: Topology B selection: Efficiencies and expected number of events for an integrated luminosity of 10.5 pb^{-1}. The efficiency for $e^+e^- \to \nu\overline{\nu}\gamma\gamma$ is defined relative to the kinematic region mentioned in the text.

$\sqrt{s}$(GeV)	$\mathcal{L}(pb^{-1})$	$N_{exp}^{\nu\overline{\nu}\gamma\gamma}$	N_{obs}
130,136	5.1	3.3	5
161	10.0	3.9	1
172	10.5	3.8	2

Table 4: Number of events expected and observed at each centre-of-mass region for the Topology C analysis.

$\sqrt{s}$(GeV)	x_1	x_2	$\cos\theta_1$	$\cos\theta_1$	ϕ_1(rad)	ϕ_2(rad)	M_{recoil}(GeV)	M_X^{max}(GeV)
130.3	0.436	0.283	0.473	-.926	4.064	1.172	81.3	52.7
130.3	0.451	0.091	0.484	0.166	2.147	4.574	91.3	25.6
136.2	0.477	0.069	-0.800	0.024	0.377	2.642	94.1	25.1
136.2	0.457	0.150	-0.420	0.896	0.692	3.408	91.7	32.0
136.2	0.517	0.070	0.466	0.413	1.413	2.484	88.3	34.1
161.3	0.403	0.166	0.580	0.095	1.206	0.581	106.9	59.5
172.0	0.594	0.171	0.046	0.787	5.509	3.776	92.6	58.7
172.0	0.566	0.209	0.901	-0.269	1.510	2.866	93.1	64.6

Table 5: Kinematic properties of the events selected by the Topology C analysis.

M_X (GeV)	Efficiency in % for topology C selection	Efficiency in % for topology C with $M_X^{max} > M_X - 5$ GeV	$\nu\overline{\nu}\gamma\gamma$ rejection efficiency (%)
45	71 ± 3	66 ± 3	46 ± 2
55	76 ± 3	72 ± 3	58 ± 2
70	78 ± 3	74 ± 3	80 ± 2
75	81 ± 3	78 ± 3	86 ± 1
80	80 ± 3	77 ± 3	94 ± 1

Table 6: Topology C selection efficiency as a function of mass for the process $e^+e^- \rightarrow XX$, $X \rightarrow Y\gamma$, and $M_Y \approx 0$. These numbers are for $\sqrt{s} = 161$ GeV. The first column shows the efficiency of the selection described in section 3.3. The second column shows the selection efficiency after the cut on M_X^{max} described in section 4.3. The final column shows the rejection efficiency of the $M_X^{max} > M_X - 5$ GeV cut for $\nu\overline{\nu}\gamma\gamma$ events.

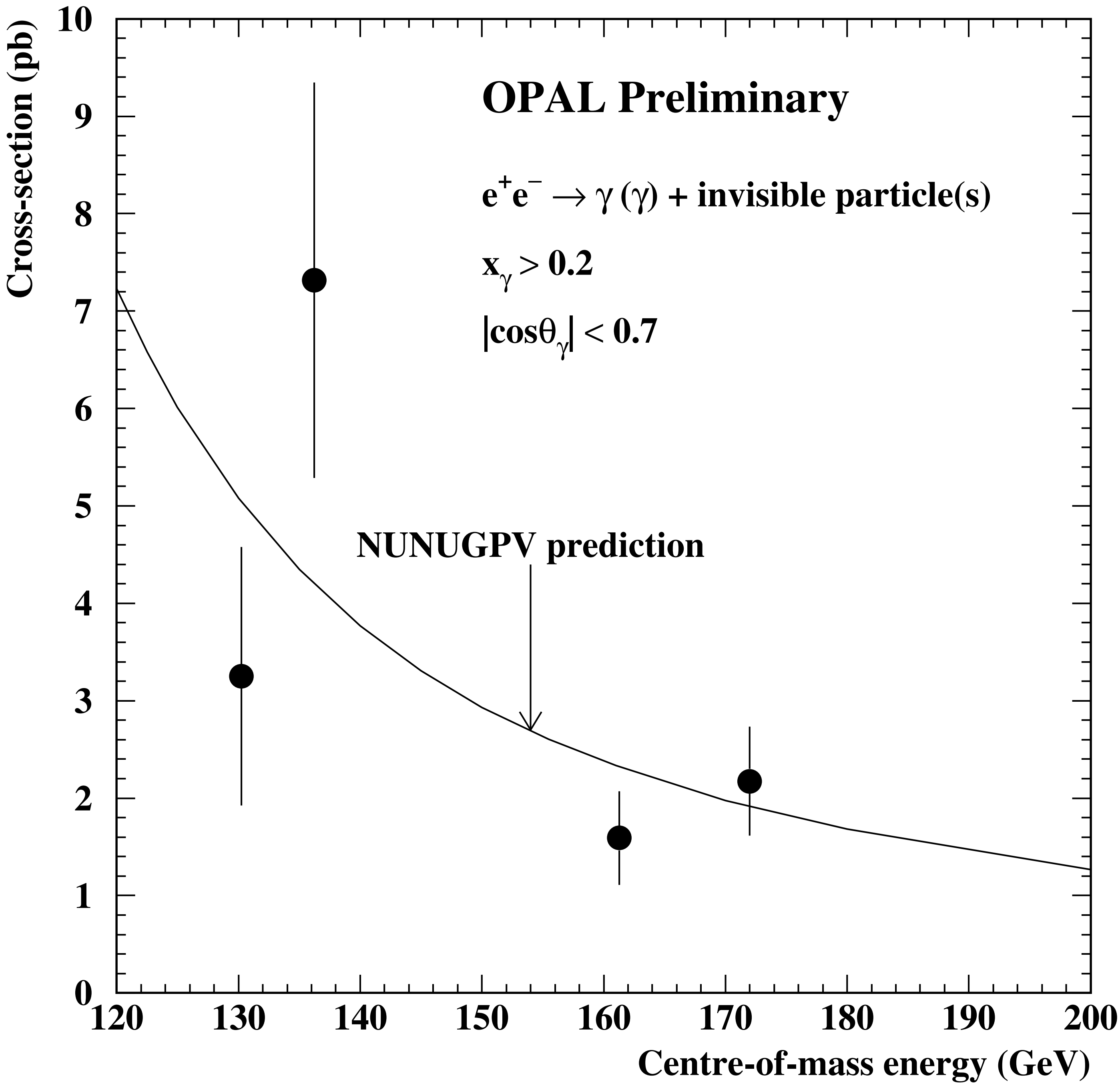

Figure 1: The measured cross-section for $e^+e^- \rightarrow \gamma(\gamma)$ + invisible particle(s) versus centre-of-mass energy. The data points with error bars are OPAL measurements from this paper and from the analysis at centre-of-mass energies of 130, 136 and 161 GeV. The curve is the Standard Model prediction for the process $e^+e^- \rightarrow \nu\bar{\nu}\gamma(\gamma)$.

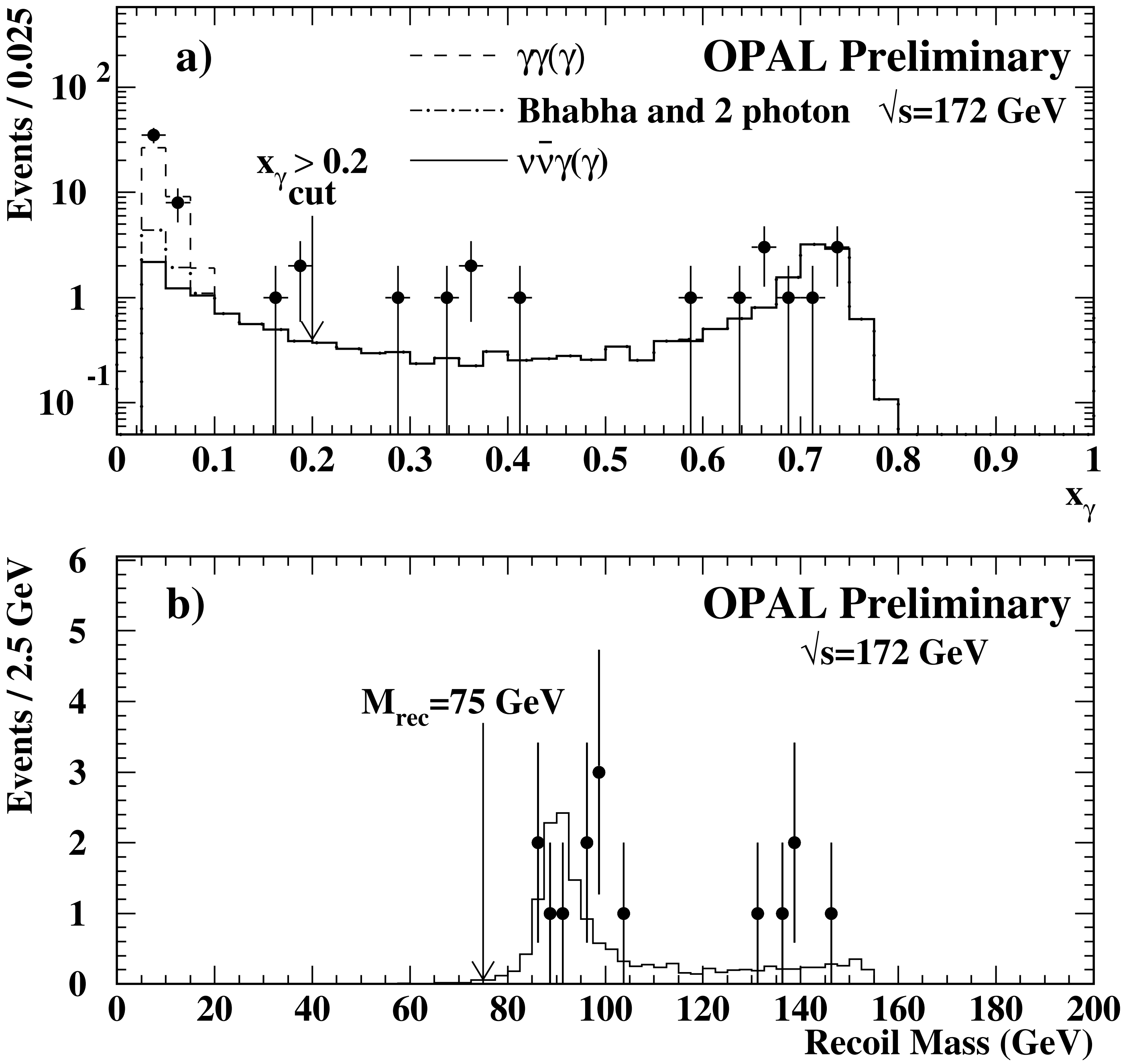

Figure 2: a) The x_γ distribution for the most energetic photon in events selected by topology A without the x_γ cut in order to show the expected background contributions at low x_γ. The data are the points with error bars, the solid line is the expected contribution from $e^+e^- \to \nu\bar{\nu}\gamma(\gamma)$ and the broken lines are the additional contribution from other Standard Model backgrounds. The Monte Carlo contributions are normalized to the 10.5 pb^{-1} of the data. b) The recoil mass distribution for selected events in topology A. The points with error bars are the data and the histogram is the expectation from the $e^+e^- \to \nu\bar{\nu}\gamma(\gamma)$ Monte Carlo normalized to the 10.5 pb^{-1} of the data.

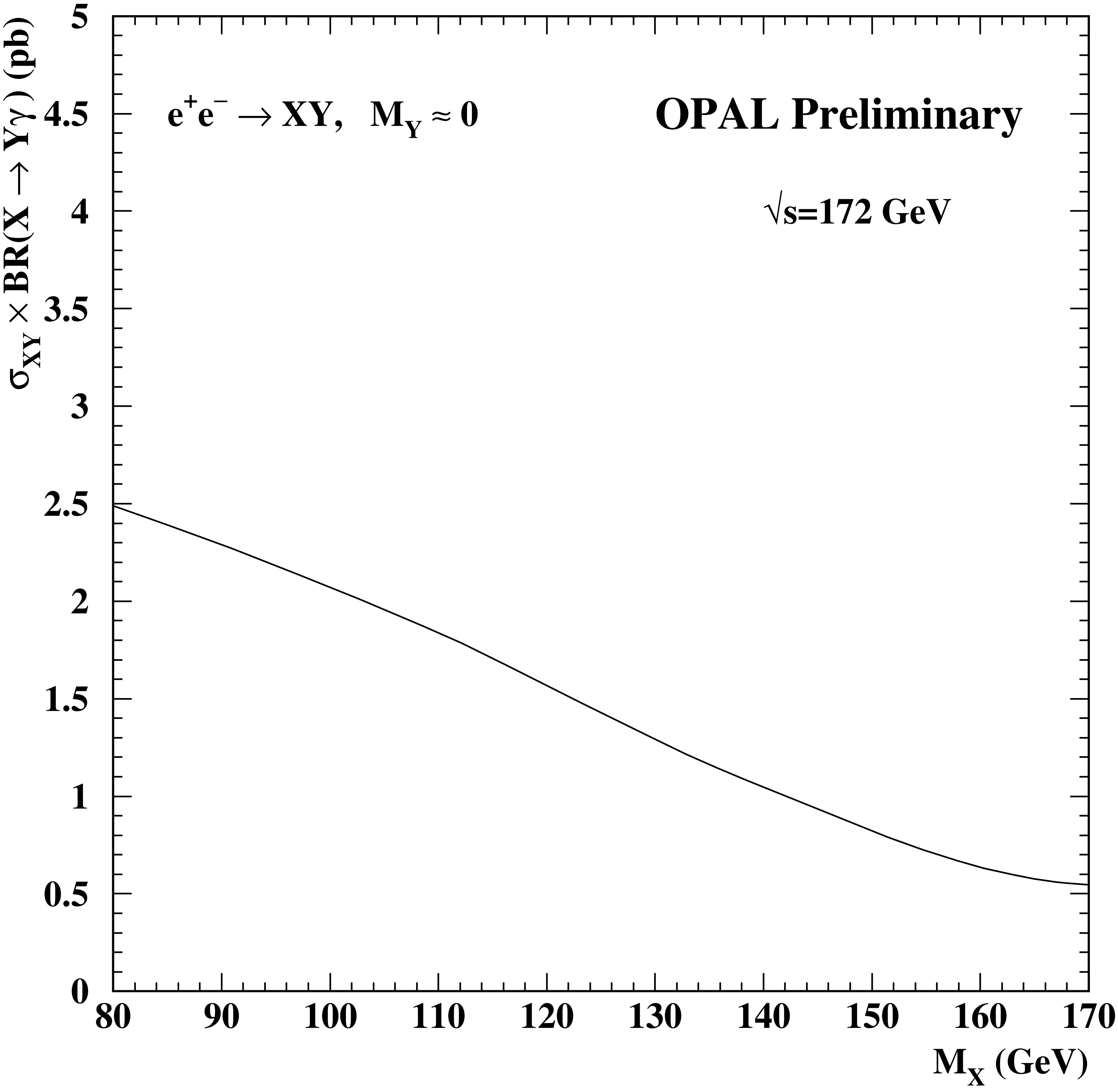

Figure 3: The 95% CL upper limit on the cross-section times the photonic branching ratio for the process $e^+e^- \to XY$, $X \to Y\gamma$ with $M_Y \approx 0$, versus M_X. This limit uses the topology A selection for one photon only and $M_{rec} < 75$ GeV.

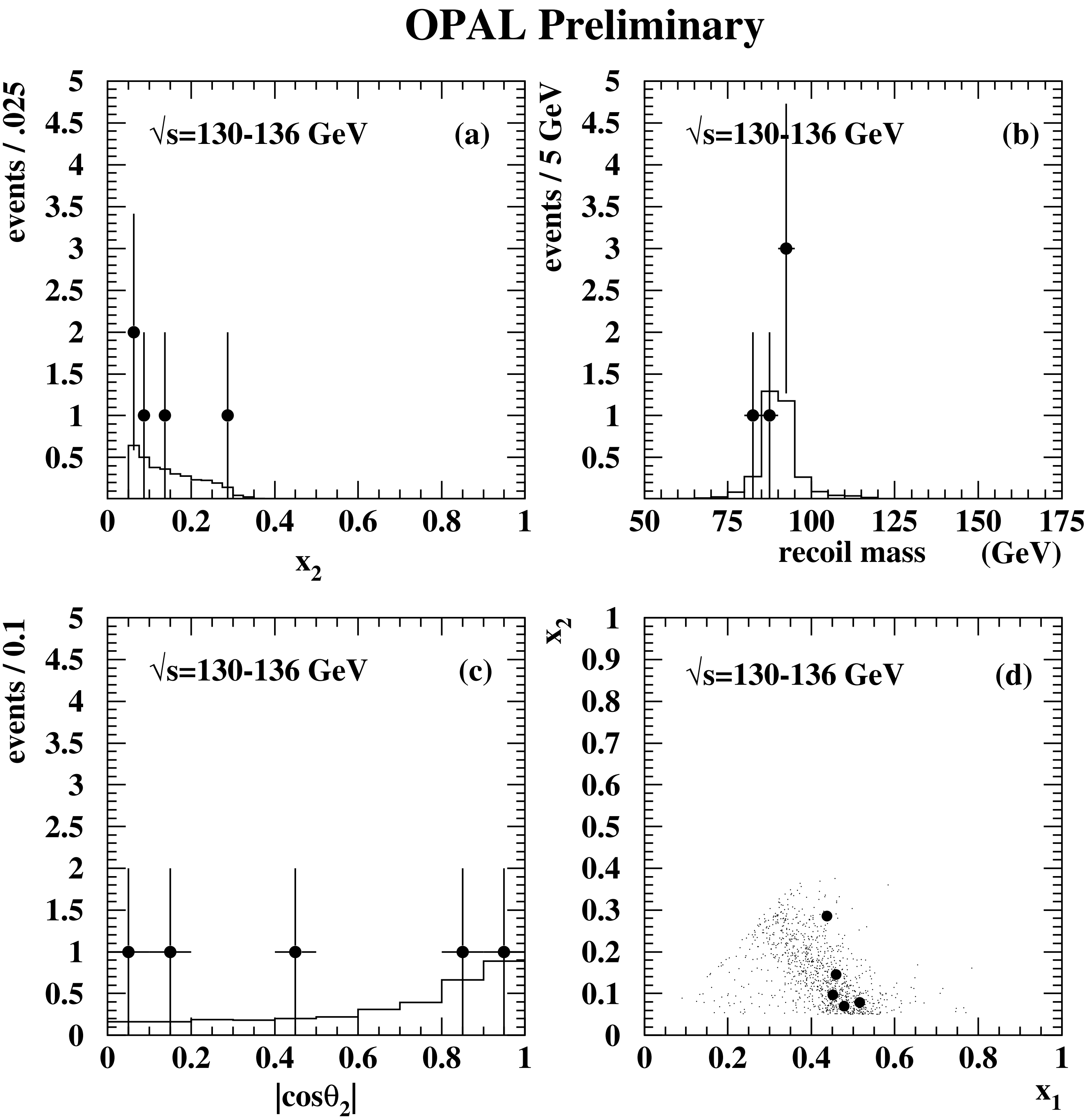

Figure 4: Results of the topology C analysis at centre-of-mass energies in the region 130-136 GeV. (a) shows the scaled energy of the least energetic photon. (b) shows the recoil mass distribution. (c) shows the polar angle distribution of the least energetic photon. (d) shows the energy of the least energetic photons plotted against that of the most energetic. In (a) to (c) the overlaid histograms represent the expected contribution from $e^+e^- \to \nu\overline{\nu}\gamma\gamma$ events, normalized to the total integrated luminosity. In (d) the overlaid scatter plot also represents the expected distribution from $e^+e^- \to \nu\overline{\nu}\gamma\gamma$ events, with arbitrary normalization.

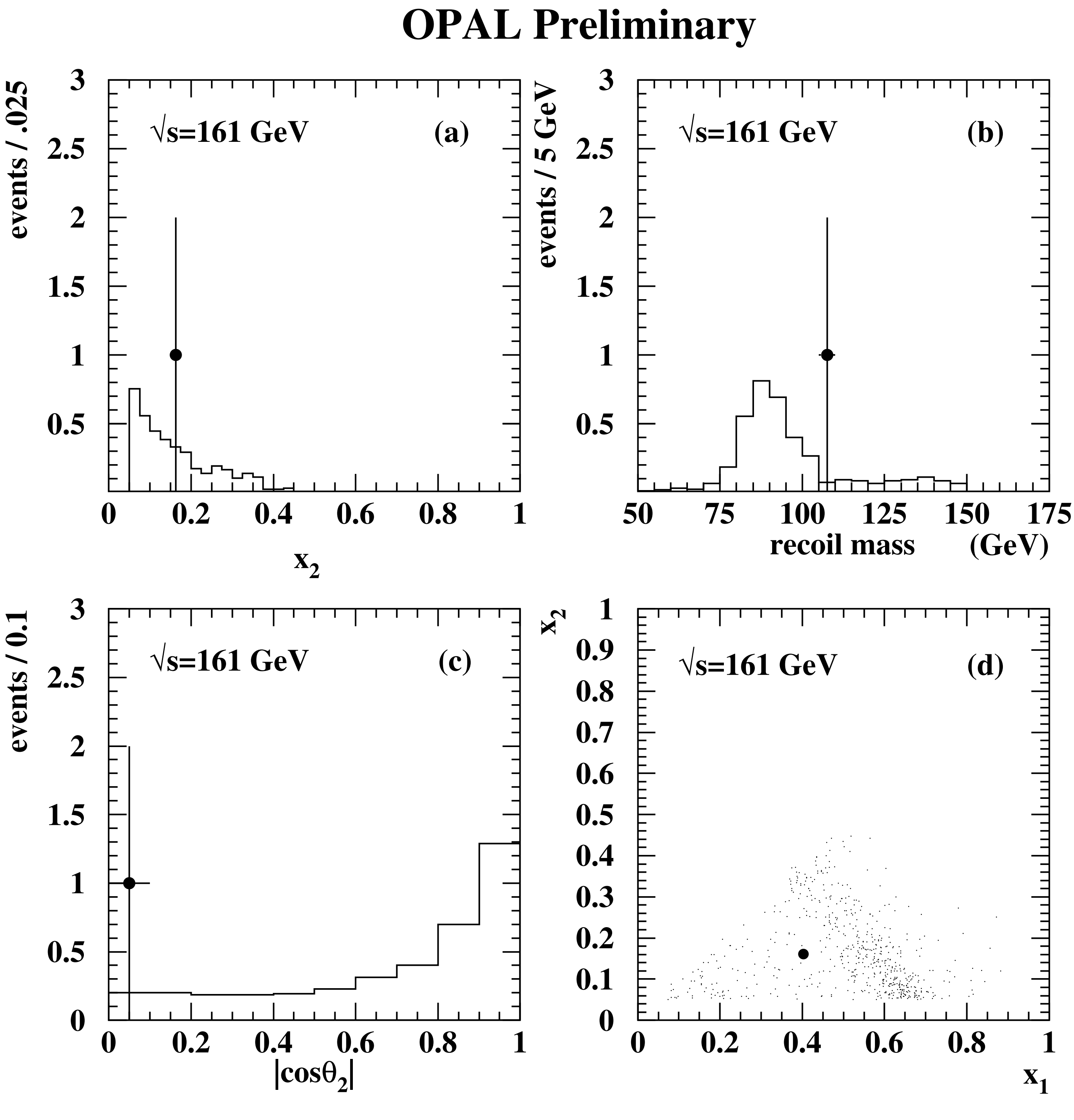

Figure 5: Results of the topology C analysis at centre-of-mass energies around 161 GeV. (a) shows the scaled energy of the least energetic photon. (b) shows the recoil mass distribution. (c) shows the polar angle distribution of the least energetic photon. (d) shows the energy of the least energetic photons plotted against that of the most energetic. In (a) to (c) the overlaid histograms represent the expected contribution from $e^+e^- \to \nu\overline{\nu}\gamma\gamma$ events, normalized to the total integrated luminosity. In (d) the overlaid scatter plot also represents the expected distribution from $e^+e^- \to \nu\overline{\nu}\gamma\gamma$ events, with arbitrary normalization.

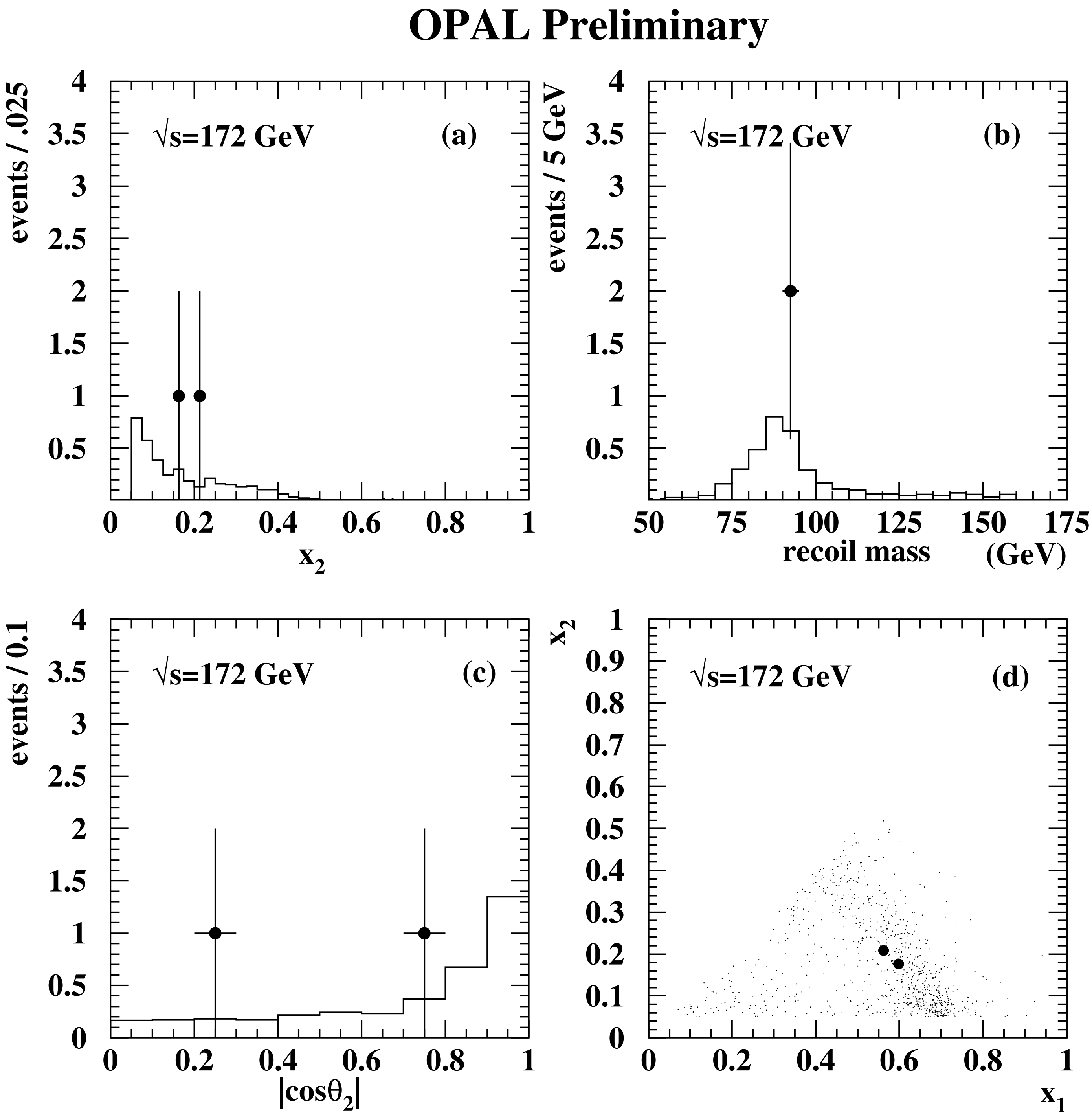

Figure 6: Results of the topology C analysis at centre-of-mass energies around 172 GeV. (a) shows the scaled energy of the least energetic photon. (b) shows the recoil mass distribution. (c) shows the polar angle distribution of the least energetic photon. (d) shows the energy of the least energetic photons plotted against that of the most energetic. In (a) to (c) the overlaid histograms represent the expected contribution from $e^+e^- \rightarrow \nu\overline{\nu}\gamma\gamma$ events, normalized to the total integrated luminosity. In (d) the overlaid scatter plot also represents the expected distribution from $e^+e^- \rightarrow \nu\overline{\nu}\gamma\gamma$ events, with arbitrary normalization.

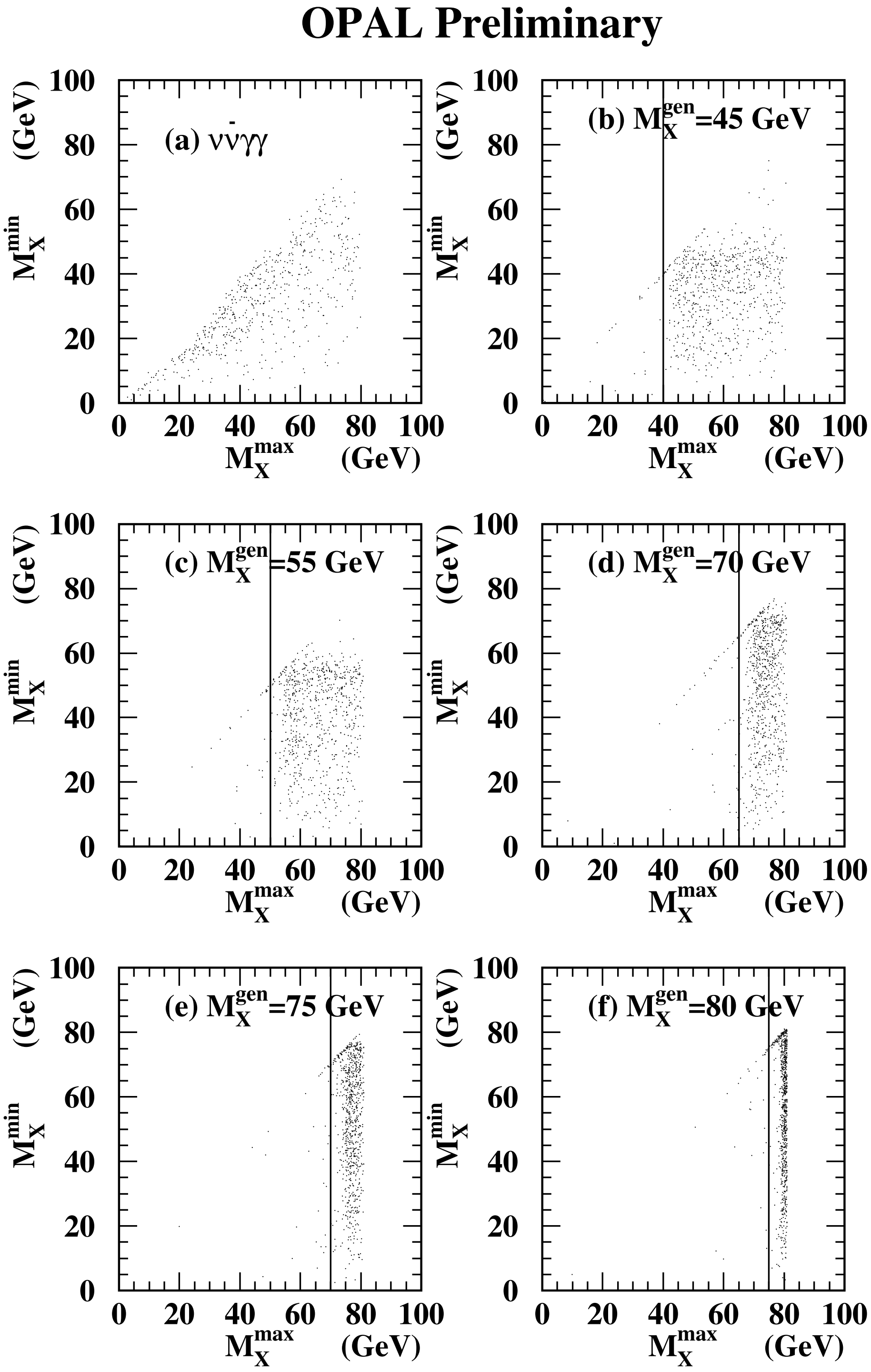

Figure 7: M_X^{min} vs. M_X^{max} for (a)$\nu\bar{\nu}\gamma\gamma$ Monte Carlo and (b)-(f) $e^+e^- \to XX$, $X \to Y\gamma$, $M_Y = 0$ Monte Carlo for various M_X. The vertical lines represent the chosen cut values discussed in the text. These are for Monte Carlo generated at a centre-of-mass energy of 161 GeV.

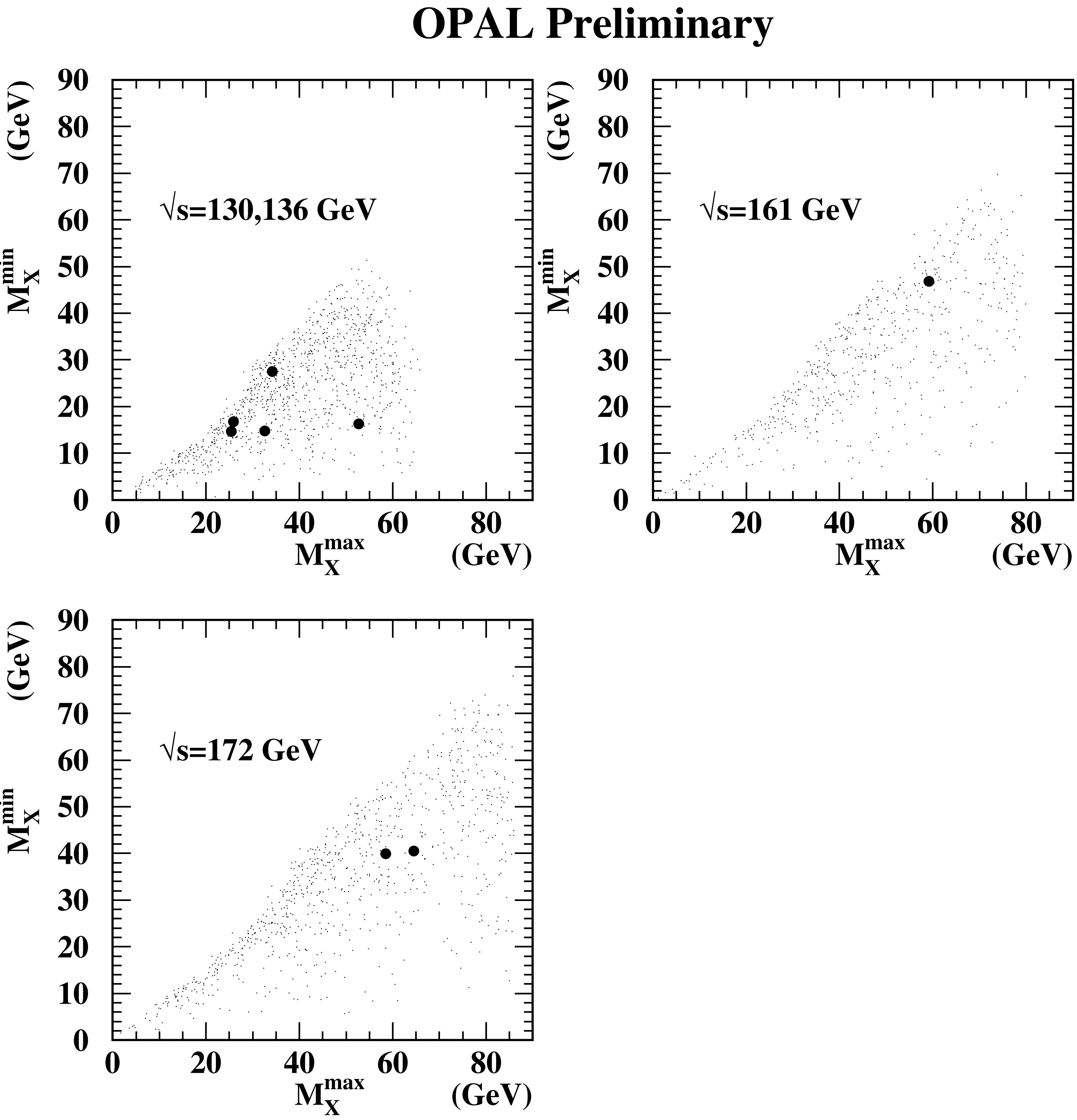

Figure 8: M_X^{min} vs. M_X^{max} for the accepted events in topology C for each centre-of-mass energy region. Overlaid are the expected distributions for contributions from the Standard Model process $e^+e^- \rightarrow \nu\overline{\nu}\gamma\gamma$.

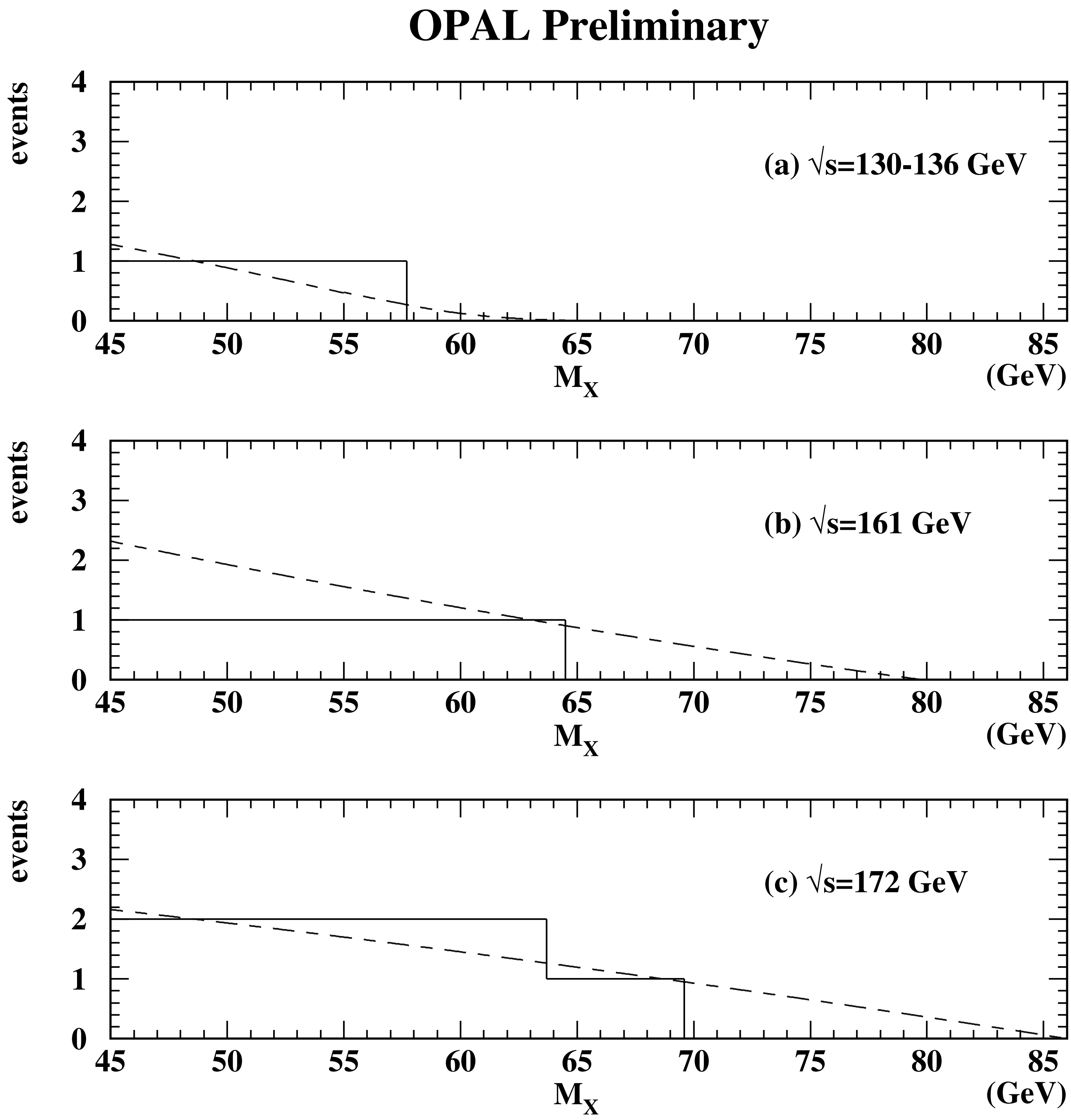

Figure 9: The number of observed candidates consistent with mass M_X (solid line) and the expected number of background events from $e^+e^- \to \nu\bar{\nu}\gamma\gamma$ (dashed line).

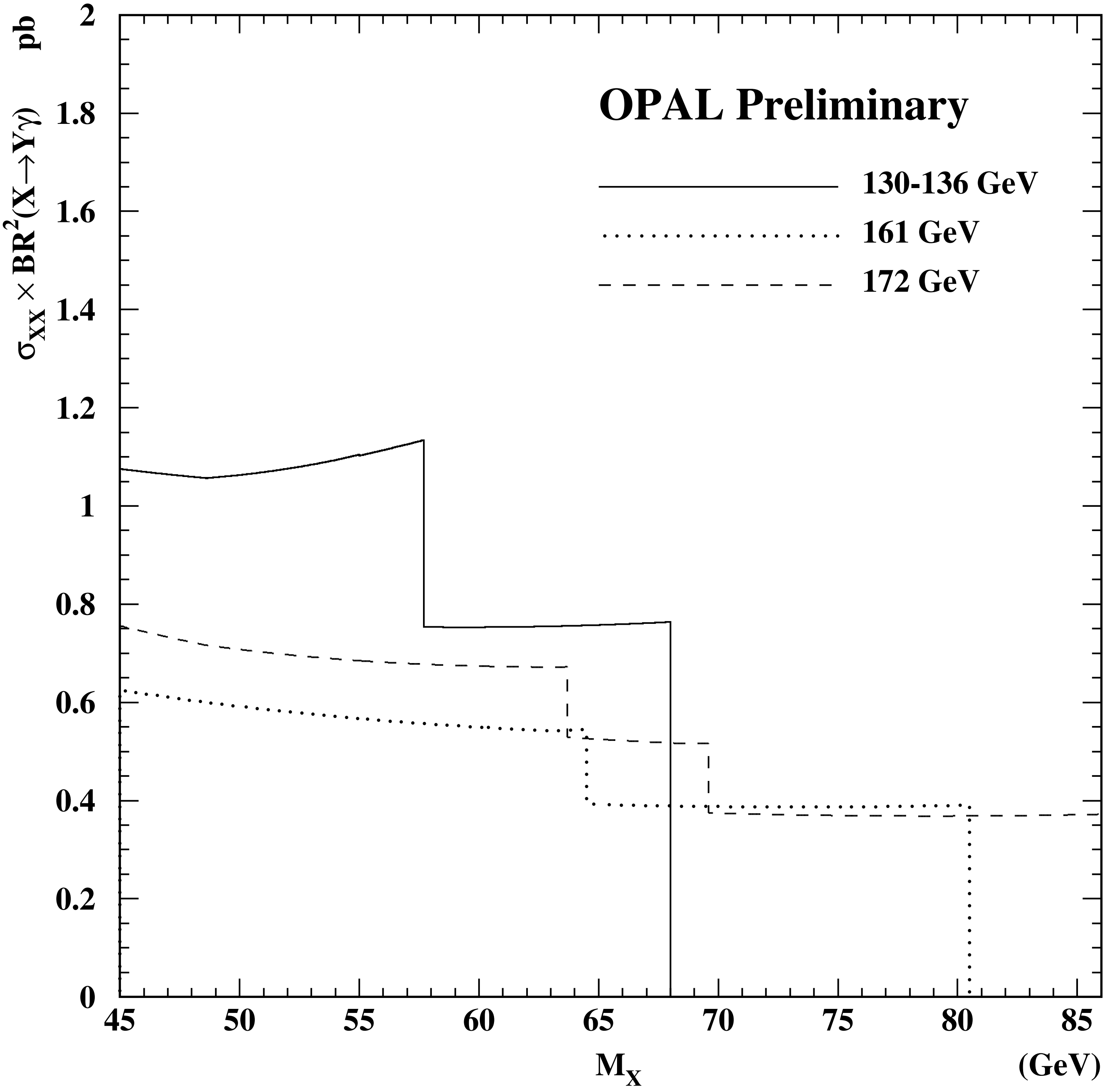

Figure 10: The 95% confidence level upper limit on the cross-section times photonic branching ratio squared for the process $e^+e^- \to XX, X \to Y\gamma$ with $M_Y \approx 0$, as a function of M_X.

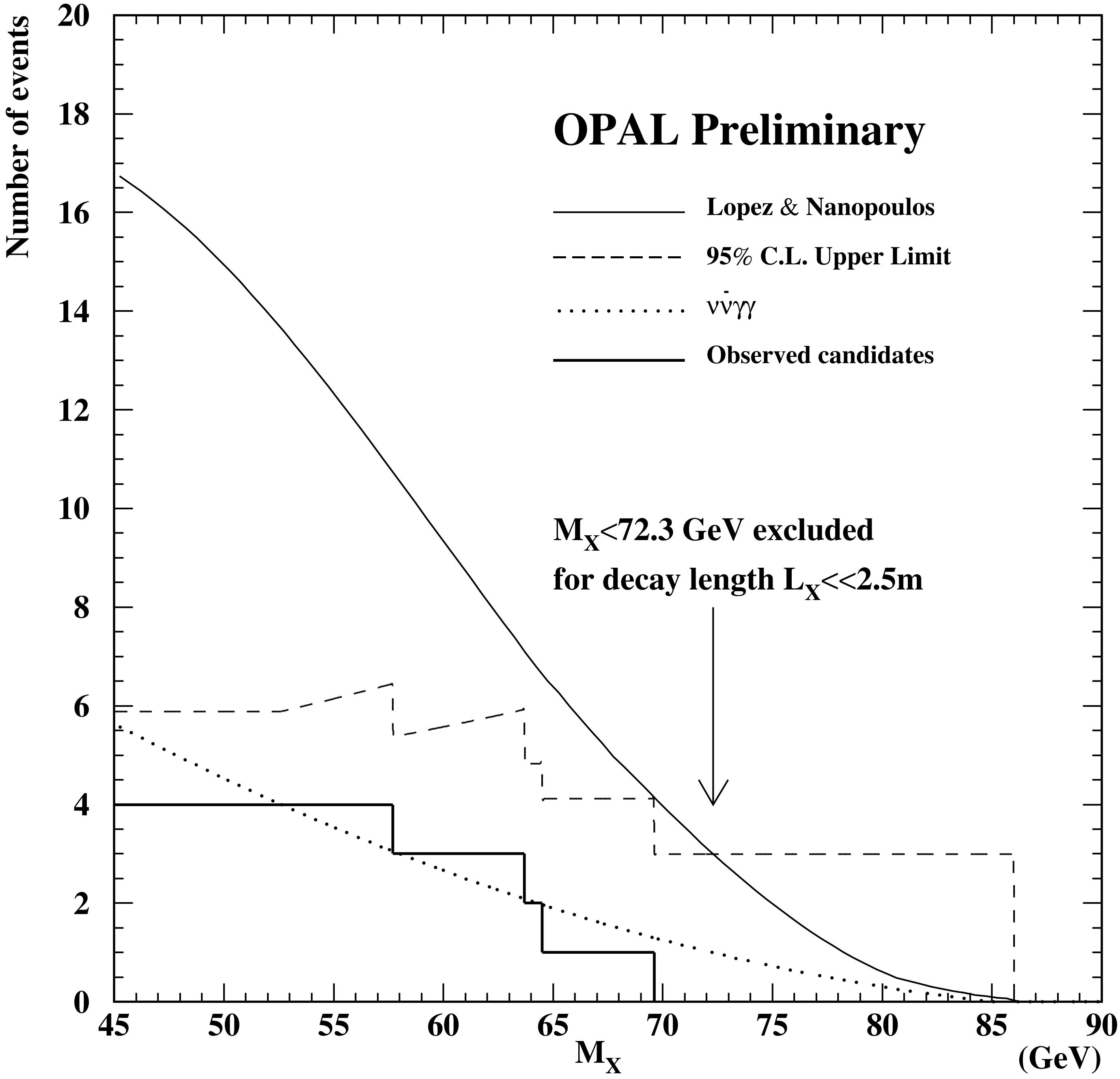

Figure 11: 95% confidence level upper limit on M_X from the combined data sample. The lower solid line shows the number of observed candidates consistent with a given value of M_X. The dotted line shows the summed expected background from $\nu\overline{\nu}\gamma\gamma$. The dashed line shows the 95% confidence level upper limit on the number of candidate events and the upper solid line shows the expected number of events from the Lopez and Nanopoulos model [14]. Within that model, values of M_X less than 72.3 GeV are excluded at the 95% confidence level, assuming a decay length L_X much less than the inner radius of the OPAL electromagnetic calorimeter (2.5m).

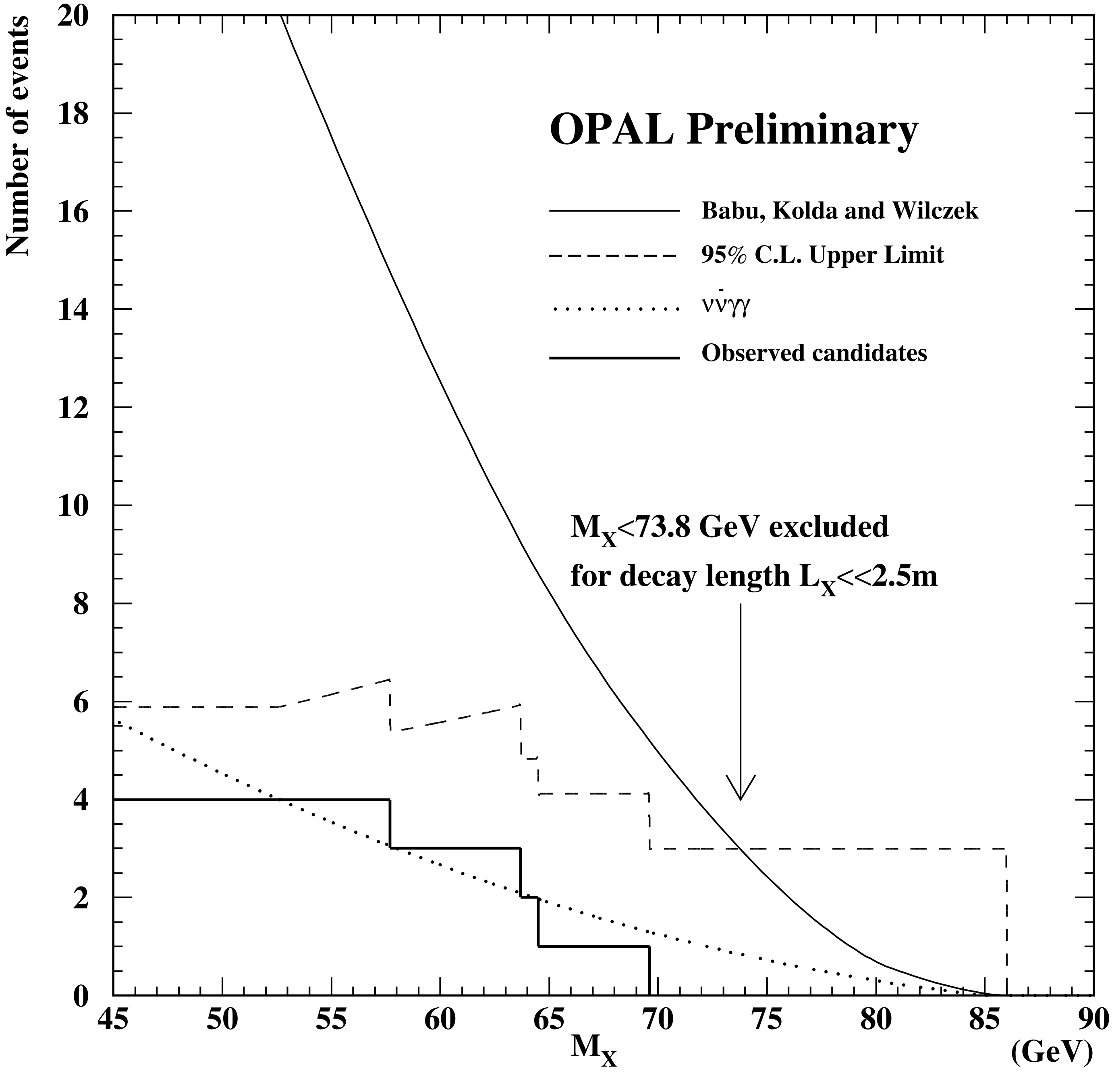

Figure 12: 95% confidence level upper limit on M_X from the combined data sample. The lower solid line shows the number of observed candidates consistent with a given value of M_X. The dotted line shows the summed expected background from $\nu\overline{\nu}\gamma\gamma$. The dashed line shows the 95% confidence level upper limit on the number of candidate events and the upper solid line shows the expected number of events from the model of Babu, Kolda and Wilczek [15]. Within that model, values of M_X less than 73.8 GeV are excluded at the 95% confidence level, assuming a decay length L_X much less than the inner radius of the OPAL electromagnetic calorimeter (2.5m).